Automatic compensation of phase aberrations in digital holographic microscopy based on sparse optimization

View Online   Export Citation   CrossMark

Zhenbo Ren,[1,a] ID Jianlin Zhao,[1] ID and Edmund Y. Lam[2,b] ID

AFFILIATIONS

[1] MOE Key Laboratory of Material Physics and Chemistry under Extraordinary Conditions, and Shaanxi Key Laboratory of Optical Information Technology, School of Science, Northwestern Polytechnical University, Xi'an 710072, China
[2] Department of Electrical and Electronic Engineering, The University of Hong Kong, Pokfulam, Hong Kong, China

Note: This paper is part of an APL Photonics Special Topic on Computational Optical Imaging.
[a] Electronic mail: zbren@nwpu.edu.cn
[b] Electronic mail: elam@eee.hku.hk

ABSTRACT

In digital holographic microscopy, phase aberrations, which are usually caused by the imperfections of components and nontelecentric configuration of the optical system, severely affect the visualization and quantitative measurement for phase-contrast imaging. Here, we propose a purely numerical and automatic method to compensate for phase aberrations. Without any manual involvement of selecting a sample-free background, the compensation is cast as a surface fitting problem, in which the aberration surface is approximated by formulating an inverse problem. By adopting the ℓ_1-norm as the loss function and by minimizing an objective function, aberrations can be accurately fitted and thus removed numerically. Synthetic and experimental results are demonstrated to verify the efficacy of this method over the least squares method.

I. INTRODUCTION

Digital holographic microscopy (DHM) is a powerful technique that can measure tiny structures such as MEMS circuits and biological specimens in real time due to its capability of recording the whole wavefront of a three-dimensional (3D) scene in a non-invasive and label-free way. By using a detector such as a CCD or a CMOS, the interference pattern between the object wave and the reference wave is recorded and stored in a digital manner. With the two-dimensional (2D) hologram, one can then numerically reconstruct the object's amplitude and quantitative phase distribution[1,2] using appropriate algorithms. By doing so, applications in tomography,[3] 3D imaging,[4] and extended focused imaging[5] have been demonstrated in recent years.

Unfortunately, a serious distortion in the quantitative phase-contrast imaging of DHM is the undesired phase aberrations. On the one hand, in the off-axis configuration, the incidence between the object beam and the reference beam illuminating onto the detector produces a constant tilt aberration, which introduces a slant to the retrieved phase. On the other hand, the microscope objective (MO), if no additional component is added to form a telecentric configuration, inevitably causes a quadratic phase aberration to the extracted phase. Besides, due to the imperfect construction of the system and alignment of components, high-order aberrations, such as astigmatism and coma, may also exist in the final image. These aberrations appearing in the phase image not only distort the visualization of the object but also severely hinder the quantitative measurement of the object's true thickness/height.[6]

In recent years, to eliminate the aberrations in the retrieved phase map, various methods have been proposed. By and large, they can be categorized into two groups: physical compensation in the optical recording stage and numerical compensation in the reconstruction stage. The former either requires additional/special optical components/configurations or demands multiple recordings. To

name a few, by adding a tube lens, a telecentric configuration is formed, and therefore, the parabolic phase is physically compensated.[7–9] The tilt phase is further removed from the phase map by a spatial filtering.[9] Similarly, by inserting an electrically tunable/adjustable lens in the illumination path or in the reference arm, the parabolic phase factor or total phase distortions can be canceled out.[10–12] Besides, a common-path interferometer with one single-cube beam splitter is also demonstrated to physically compensate phase aberrations.[13] As for the latter scheme of multiple recordings, although the double exposure method is capable of eliminating all of the aberrations, a second object-free reference hologram has to be captured.[14,15] Under some situations, even two more laterally shifted holograms have to be collected.[16] As such, these methods are only appropriate for static scenarios. All in all, the physical compensation strategy complicates the holographic recording and makes it more bulky.

Another group of compensation methods, as mentioned above, is based on numerical postprocessing. Roughly speaking, fitting-based numerical methods involve in the use of different polynomials such as standard polynomials,[17,18] digital phase mask,[19,20] and Zernike polynomials.[17,21] By solving a least-squares problem[19,21] or a phase variation minimization problem,[20] the aberration surface is thus fitted and then subtracted from the phase map, resulting in a pure object phase finally. Comparatively, nonfitting methods employ various mathematical models and special operations on the hologram. For example, Zuo *et al.* used principal component analysis (PCA) to decompose the phase map into a set of values of uncorrelated variables, thus extracting aberration terms from the first principal component obtained.[22] A method that analyzes the frequency spectrum of a hologram for aberration removal is also demonstrated.[23,24] Besides, a hologram rotation-based method is proposed, in particular, for getting rid of the off-axis tilt as well as the parabolic phase aberration.[25,26]

Despite the success and flexibility of current numerical approaches, manual operations of selecting a flat region as reference surfaces[17,19] are required, an assumption is made that the object is so thin that it is just a small perturbation in the aberration contribution to the overall reconstructed phase distribution,[18,21] or only low-order aberrations such as the phase curvature introduced by the MO can be removed.[18] It is worth noting that the polynomial-based method is a semiautomatic method since it requires background information to find the phase residual, which is detected by manually cropping a flat background area as Refs. 17 and 19. Besides, although PCA can automatically predict the phase residual by creating a self-conjugated phase to compensate aberrations and can be extended to deal with high-order aberrations, it assumes that only noncross terms exist, limiting the scope of this method.[22,27] Furthermore, manual filtering and centering[23] or hypothesis of a thin phase object[24] is inevitable in the spectrum-based analysis, and the self-hologram rotation is solely suitable for tilt aberration compensation.[25] Recently, a learning-based method is proposed to automatically detect the specimen-free background for the subsequent fitting using Zernike polynomials.[28] Aberration removal is further encapsulated in holographic reconstruction and thus can be automatically compensated during the feed-forward propagation along the network.[29] Despite its success and applicability to high-order aberrations, the learning-based method requires a lot of data and extensive computation for network training.

In this paper, we propose a purely numerical method that can remove phase aberrations of any orders in a totally automatic manner for DHM. By formulating the surface fitting as an inverse problem and by solving an ℓ_1-norm-based optimization, the aberration surface can be accurately estimated and a high-quality aberration-free quantitative phase-contrast image is then recovered. Synthetic and experimental results of multiple samples are demonstrated to verify the efficacy of the proposed method.

II. METHOD

On the reconstruction plane (x, y), based on the recovered complex wavefront $\Gamma(x, y)$, the unwrapped and phase map is extracted by

$$\phi(x,y) = \text{UNWRAP}\left[\arctan\left(\frac{\text{Im}[\Gamma(x,y)]}{\text{Re}[\Gamma(x,y)]}\right)\right], \quad (1)$$

where UNWRAP[·] indicates the phase unwrapping operation and Re and Im denote the real and imaginary parts, respectively. Under situations that no physical compensation is implemented, taking aberrations into account, the recovered phase is the summation of the object phase and the aberration, which reads

$$\phi(x,y) = \phi_{obj}(x,y) + \phi_{abe}(x,y), \quad (2)$$

where $\phi_{obj}(x, y)$ is the object phase distribution and $\phi_{abe}(x, y)$ is the total aberration term overlapping with $\phi_{obj}(x, y)$. The purpose of numerical aberration compensation is *to find an approximation*, $\hat{\phi}_{abe}(x,y)$, *of the real aberration* $\phi_{abe}(x, y)$ *as accurately as possible*. As such, the aberration-free object phase can be then fully recovered by

$$\hat{\phi}_{obj}(x,y) = \phi(x,y) - \hat{\phi}_{abe}(x,y)$$
$$\approx \phi_{obj}(x,y). \quad (3)$$

In order to approximate the aberration, a theoretical fitting model is necessary. According to the principle of homogeneous polynomial fitting, the surface model we are using here is in second-order and can be written as

$$\hat{\phi}_{abe}(x,y) = \beta_1 x^2 + \beta_2 y^2 + \beta_3 xy + \beta_4 x + \beta_5 y + \beta_6, \quad (4)$$

where β_i, $i = 1, \ldots, 6$, denote the fitting coefficients to be estimated. Note that for mathematical simplification, the model we show here is second-order. This illustrates that the commonly occurred aberrations in DHM, such as tilt, astigmatism, and parabolic surface, can be successfully compensated using this fitting model. However, the extension of the fitting model to higher order is straightforward without any further efforts if high-order aberrations have to be removed.

With the help of the fitting model, we can then proceed to estimate its coefficients, which determines the aberration surface. To do so, by assuming that the object phase is a small perturbation compared to the aberration (this is a reasonable hypothesis for the situations in DHM[18,21]), we can rewrite $\phi(x,y) = \hat{\phi}_{abe}(x,y)$ in the matrix notion as

$$
\begin{bmatrix}
x_1^2 & y_1^2 & x_1 y_1 & x_1 & y_1 & 1 \\
x_2^2 & y_2^2 & x_2 y_2 & x_2 & y_2 & 1 \\
\vdots & \vdots & \vdots & \ddots & \vdots & \vdots \\
x_n^2 & y_n^2 & x_n y_n & x_n & y_n & 1
\end{bmatrix}
\begin{bmatrix}
\beta_1 \\ \beta_2 \\ \beta_3 \\ \beta_4 \\ \beta_5 \\ \beta_6
\end{bmatrix}
=
\begin{bmatrix}
b_1 \\ b_2 \\ \vdots \\ b_n
\end{bmatrix},
\tag{5}
$$

where $\vec{\beta} = (\beta_1, \beta_2, \ldots, \beta_6)^T$ denotes the coefficients, $\vec{b} = (b_1, b_2, \ldots, b_n)^T$ denotes the phase $\phi(x, y)$, and n is the number of pixels of the phase image. Suppose that A denotes the matrix of the polynomials, Eq. (5) is written as

$$
A\vec{\beta} = \vec{b}.
\tag{6}
$$

This is a typical inverse problem, which is usually ill-posed. Conventionally, this problem is solved by the least squares method, in which the residual between the actual value and the value predicted by the model is minimized with the ℓ_2-norm loss function.[18] Instead, to seek the estimation of $\vec{\beta}$, by incorporating regularization technique, which is a process of introducing additional information in order to prevent overfitting, the objective function we propose to minimize is

$$
f(\vec{\beta}) = \| A\vec{\beta} - \vec{b} \|_1 + \lambda \| \vec{\beta} \|_1,
\tag{7}
$$

where $\| \cdot \|_1$ denotes the ℓ_1-norm and λ is a regularization parameter determined by trial and error. Then, by solving Eq. (7), the fitting coefficients can be acquired by

$$
\hat{\vec{\beta}} = \arg\min_{\vec{\beta}} f(\vec{\beta}).
\tag{8}
$$

Therefore, after having a proper approximation of $\vec{\beta}$, according to Eq. (4), an estimated phase aberration $\hat{\phi}_{abe}(x, y)$ can be obtained. By using Eq. (3), an aberration-free object phase distribution can then be recovered for visualization and quantitative measurement. The process is totally automatic since no flat region has to be selected as the reference in our method. The only necessary information is the recovered phase image with aberration, which is always available.

To explain why changing from the ℓ_2-norm to ℓ_1-norm can improve the fitting accuracy, we turn to the well-known compressed sensing theory. As is well known, the least squares method for regression analysis is to minimize an ℓ_2-norm loss function. As such, this optimization problem is equal to minimizing the amount of energy in the system and is mathematically simple to solve. However, such a formulation leads to poor fitting results for many practical applications for which the unknown coefficients have nonzero energy. Instead, to enforce the sparsity constraint when solving linear equations, one can minimize the number of nonzero components of the solution, which is the so-called ℓ_0-norm in a broad sense.[30] This means that finding the sparsest solution x, which is feasible to sensing constraints given by the encoding matrix A and the observation vector b, can be summarized as an ℓ_0 minimization problem. Furthermore, in mathematics, it has been proved that for many problems such as the compressive imaging problem here, the ℓ_1-norm can be used *in lieu* of the ℓ_0-norm. Consequently, one can solve the ℓ_1 problem instead of the ℓ_0 problem since the former is less difficult and easy to solve mathematically.[31,32] Therefore, formulating an ℓ_1-norm loss function has a better performance than the ℓ_2-norm for our case.
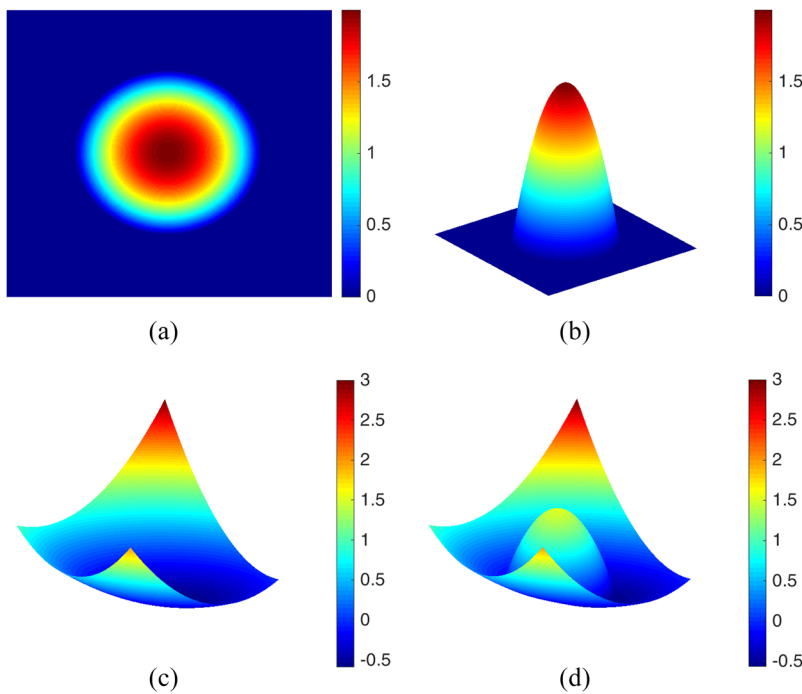

FIG. 1. Simulated object phase in (a) 2D and (b) 3D. (c) Simulated phase aberration with the first 6 terms of the Zernike polynomials. (d) Object phase overlapped with aberration. The unit of the color bar is radian.

III. SYNTHESIZED AND EXPERIMENTAL RESULTS

A. Simulation

We first test the proposed method on synthesized data, which is implemented on a PC with Intel Xeon W-2145 at 3.70 GHz and 64 GB RAM. Figures 1(a) and 1(b) present a computer-generated phase map with a size of 256 × 256 on a flat background in 2D and 3D visualizations, respectively. In Fig. 1(c), a synthetic phase aberration is generated using the first 6 terms of the Zernike polynomials,[21] leading to tilt aberration in the x and y axes, astigmatism at 0° and 45°, and defocus. The coefficients used in the simulation are given in Table I. By adding up the object phase and aberration, an aberration-distorted phase is then created and shown in Fig. 1(d).

To remove the phase aberration, the proposed ℓ_1-norm method and conventional least squares method are employed separately and solved using the SDPT3 4.0 algorithm,[33] and the compensated results are shown in Fig. 2. As can be seen, with the

TABLE I. Simulated aberrations using Zernike polynomials.

Order	Form	Description	Coefficients
0	1	Piston	0.0
1	y	Tilt at x	0.0
2	x	Tilt at y	0.5
3	$-1 + 2x^2 + 2y^2$	Defocus	0.5
4	$2xy$	Astigmatism at y	0.5
5	$x^2 - y^2$	Astigmatism at x	0.0

ℓ_1-norm-based optimization, the aberration is totally removed and the recovered object phase has exactly the same phase range to the original one, while the conventional method gives an inaccurate compensated background. This can be further observed by the quantitative comparison of phase profiles across the individual
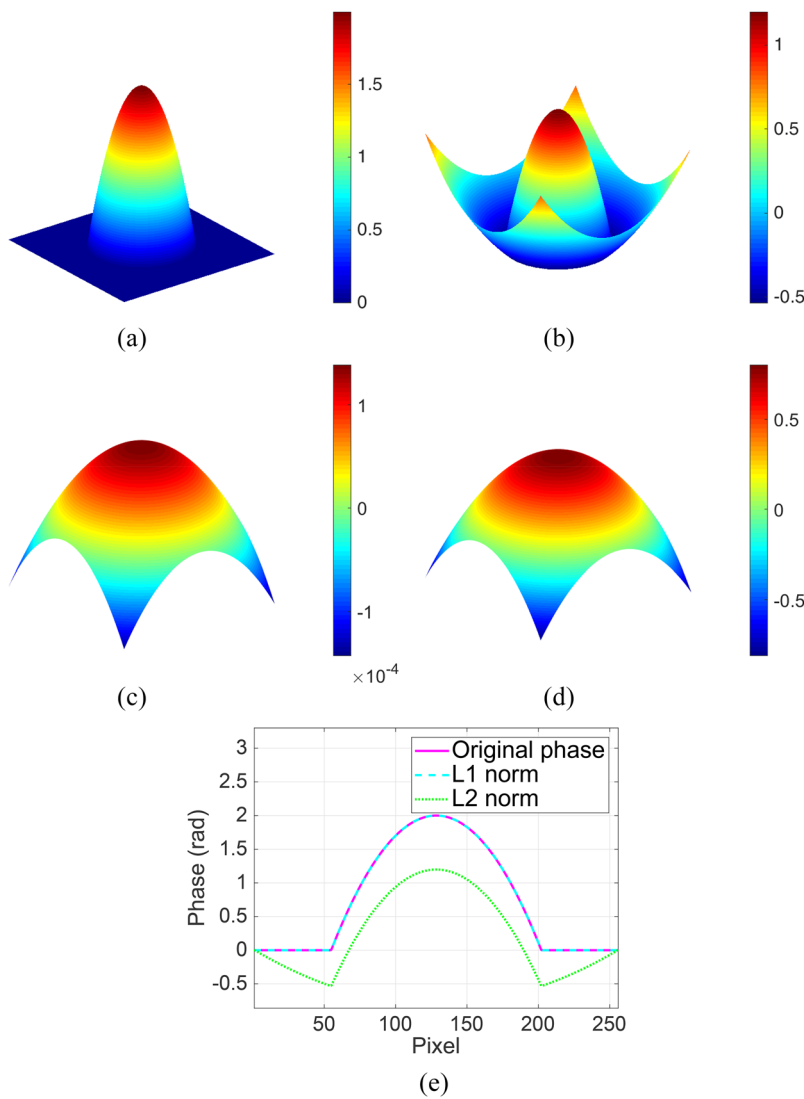

FIG. 2. Compensated phase using (a) ℓ_1 optimization and (b) conventional least squares method. Error maps of (c) ℓ_1 optimization and (d) conventional least squares method. (e) Comparison of phase profiles along the central line in (a) and (b).
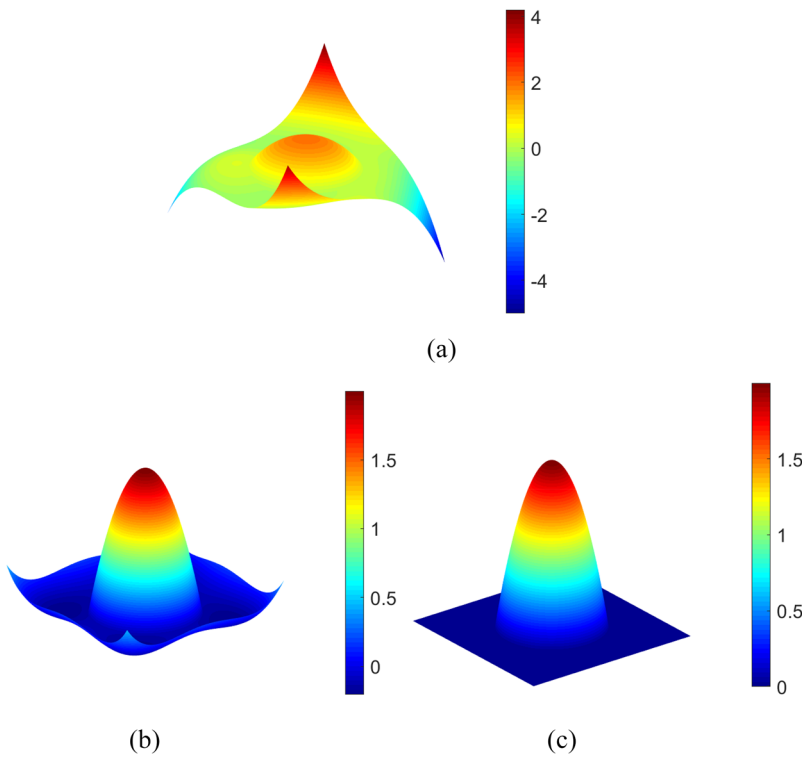
(a)

(b)

(c)

FIG. 3. (a) Generated high-order aberration. (b) Compensated result using ℓ_1-norm-based method. (c) Compensated result using the least-squares method.

central lines in Fig. 2(e). As such, the superior performance of the proposed method can be verified.

To illustrate the capability of the proposed method in high-order aberration removal, we use the same phase object in Fig. 1(b)

and generate a high-order aberration with the first 16 Zernike terms and the aberration is shown in Fig. 3(a). Suppose that a fourth-order fitting model is adopted, then Eq. (4) is written as
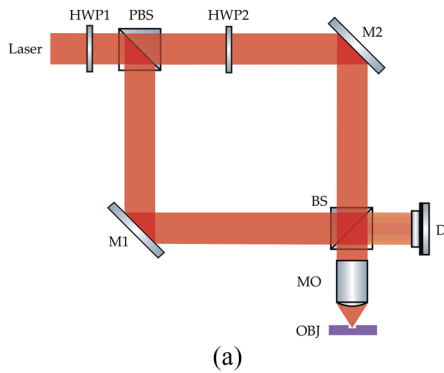

(a)

(b)

(c)

FIG. 4. (a) DHM setup operating in reflection mode. HWP1 and HWP2 are the half-waveplates. PBS and BS are the polarization and nonpolarization beam splitters, respectively. M1 and M2 are the mirrors. MO is the microscope objective lens. OBJ is the object. D is the detector. (b) Groove, as indicated by the red arrows. Only one groove is imaged in the following experiment. (c) Microcircuit.
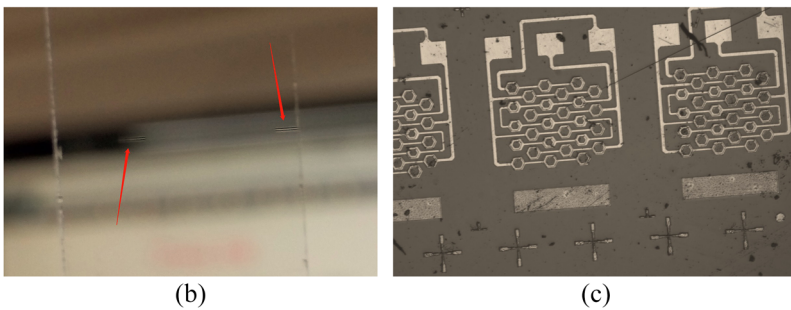
$$\hat{\phi}_{abe}(x,y) = \beta_1 x^4 + \beta_2 y^4 + \beta_3 x^3 y + \beta_4 xy^3 + \beta_5 x^2 y^2 + \beta_6 x^3$$
$$+ \beta_7 y^3 + \beta_8 x^2 y + \beta_9 xy^2 + \beta_{10} x^2 + \beta_{11} y^2 + \beta_{12} xy$$
$$+ \beta_{13} x + \beta_{14} y + \beta_{15}. \tag{9}$$

Based on this model, we use the ℓ_1-norm-based method and the least squares method for compensation. The results are given in Figs. 3(b) and 3(c), respectively. As can be clearly seen, the conventional method can basically work in this case. However, the bottom plane is not flat and contains fluctuation, which would introduce errors in the calculation of the object phase. While the proposed method can give a pretty flat bottom plane as well as a precise compensated result. The synthesized result here demonstrates an intuition of the convenience of extending the proposed method to higher-order aberration compensation.

B. Experiment

We further demonstrate the performance of this method using experimental data. The DHM system, as shown in Fig. 4(b), used to acquire data is an off-axis Mach-Zehnder interferometer with a 4X MO (GCO-2101, L = 45 mm, Daheng Optics) working in the reflection mode. The wavelength of the He–Ne laser source is 632.8 nm, and the pixel pitch of the detector (MER-130-30UM-L, 1280 × 1024 pixels, Daheng Imaging) is 5.2 μm. Two samples, a groove etched on an optical wafer shown in Fig. 4(c) and a microcircuit on a sapphire wafer shown in Fig. 4(d), are used as objects.[34] The collimated laser beam is split by the PBS and enters the interferometer along two paths. The reference beam, which is reflected by M1, directly goes into the detector, while another beam, which is reflected by M2, focuses onto the OBJ through the MO and illuminates the sample. Then, the object beam, which is the beam reflected by the sample, goes back to the detector. Two beams interfere and lead to an

(a)
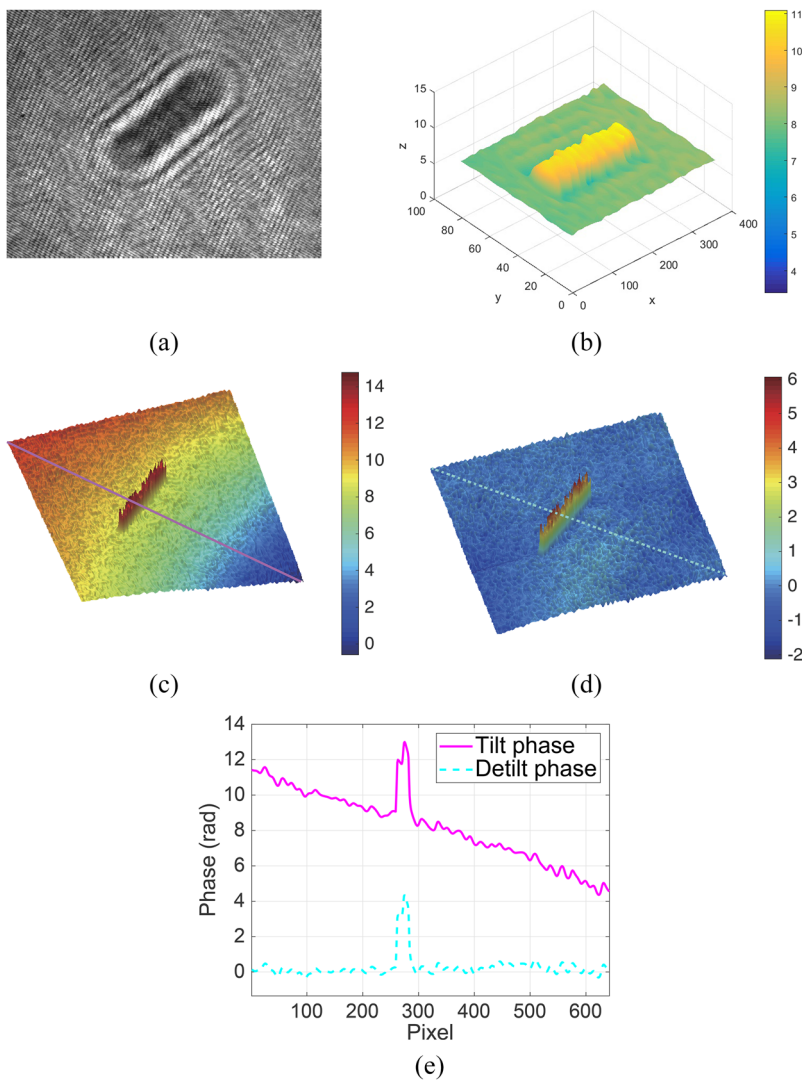

(b)

(c)

(d)

(e)

FIG. 5. (a) Hologram of the groove. (b) True groove phase acquired with a different DHM setup. (c) Recovered object phase with tilt aberration. (d) Compensated object phase. (e) Line profile comparison along diagonals in (c) (red dashed line) and (d) (blue solid line).

interference pattern, which is the hologram and is collected by using the detector. The PBS and two HWPs are designed to collaboratively change the polarization state, leading to the interference of two beams as well as the adjustment of the contrast of the interference pattern. Since it is challenging to intentionally create specific aberrations in the experiment, in this section, removal of two commonly occurred aberrations in DHM, tilt aberration and quadratic aberration, is demonstrated.

1. Removal of linear aberration

To ensure only tilt aberration is remained, the quadratic aberration introduced by the MO is optically corrected with the telecentric configuration.[8,35] In Fig. 5(a), the hologram of the groove is presented, and for a clear comparison, a *true* groove phase shown in Fig. 5(b) is acquired with a totally new DHM setup. All hardwares and configurations are different from our system used here. For a better visualization, the acquired phase map is cropped and magnified properly. Figure 5(c) shows the recovered phase image with aberration. As can be clearly seen, the groove is located on a tilt

plane, even with some astigmatism at corners, while in Fig. 5(d), the tilt surface is successfully removed using the proposed method, and the absolute height of the groove can be thus easily measured according to the difference of the groove and the flat surface. Profiles of the individual diagonals in the aberrated and corrected phase images are also demonstrated in Fig. 5(e) for comparison. The true phase of the groove can therefore be measured as around 4 rad. Another example, as shown in Fig. 6, presents the tilt aberration removal for the sample circuit. Figure 6(a) shows the hologram of the circuit, and the *true* circuit phase is given in Fig. 6(b). Similarly, the recovered phase in Fig. 6(c) has a tilt distortion, while in Fig. 6(d), the slope is removed such that the true phase of the circuit can be measured. Figure 6(e) compares the phase profiles along central lines in the two phase images.

2. Removal of quadratic aberration

As for the compensation of quadratic aberration, we first capture a hologram of the groove without telecentric configuration, leading to the introduction of quadratic curvature. Figure 7(a)
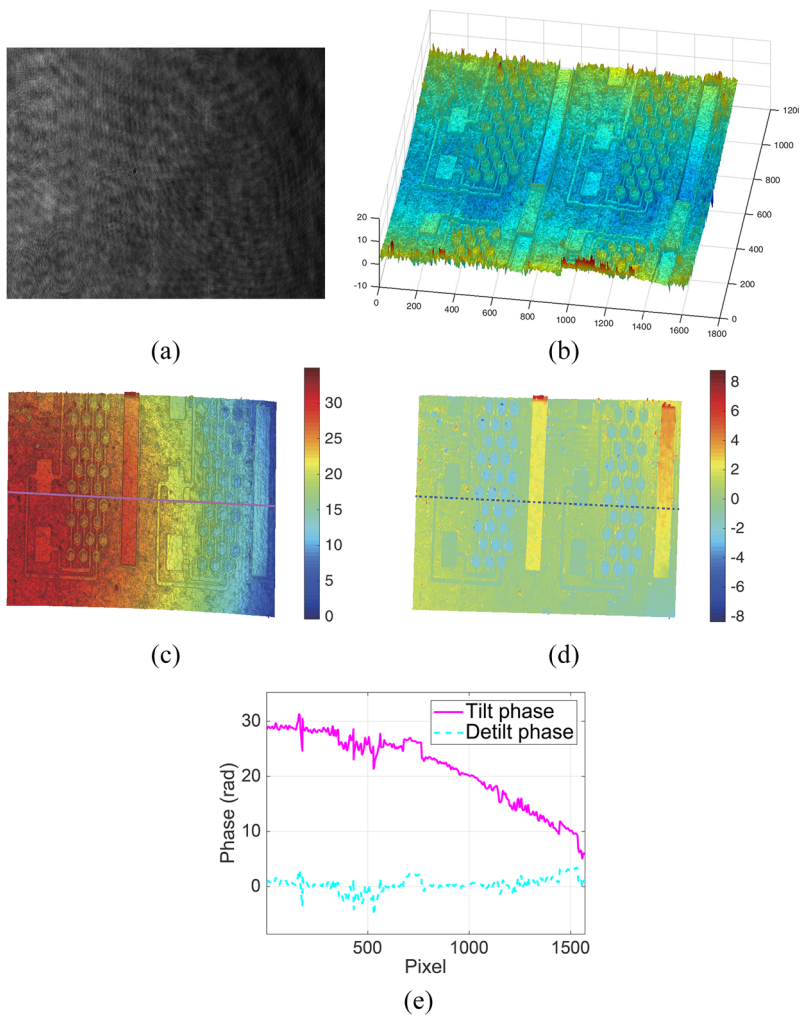

(a)

(b)

(c)

(d)

(e)

FIG. 6. (a) Hologram of the circuit. (b) True circuit phase acquired with a different DHM setup. (c) Recovered object phase with tilt aberration. (d) Compensated object phase. (e) Line profile comparison along central lines in (c) (red dashed line) and (d) (blue solid line).
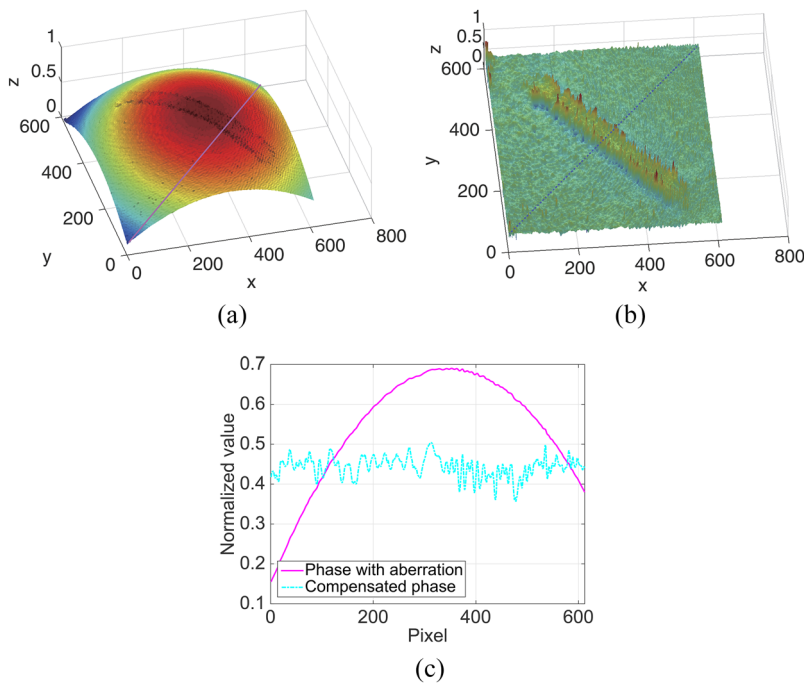
(a)

(b)

(c)

FIG. 7. (a) Recovered object phase with quadratic aberration. (b) Compensated object phase. (c) Normalized phase profiles [red dashed line in (a) and blue solid line in (b)] for comparison.

shows the recovered phase-contrast image in which the object phase is overlapped with a quadratic surface. The curvature, as can be seen clearly, introduced by the MO significantly hinders the measurement of the true thickness of the object. By using the proposed method, in Fig. 7(b), however, the quadratic surface is eliminated and the groove is thus located on a flat plane. From

Fig. 7(c), we can see that removal of the notorious quadratic surface in phase imaging benefits the quantitative measurement of the object. Then, with the telecentric configuration, holograms of the groove and the circuit are collected. Note that although in theory, parabolic aberration should be removed in such configurations. However, due to the misalignment of components, the
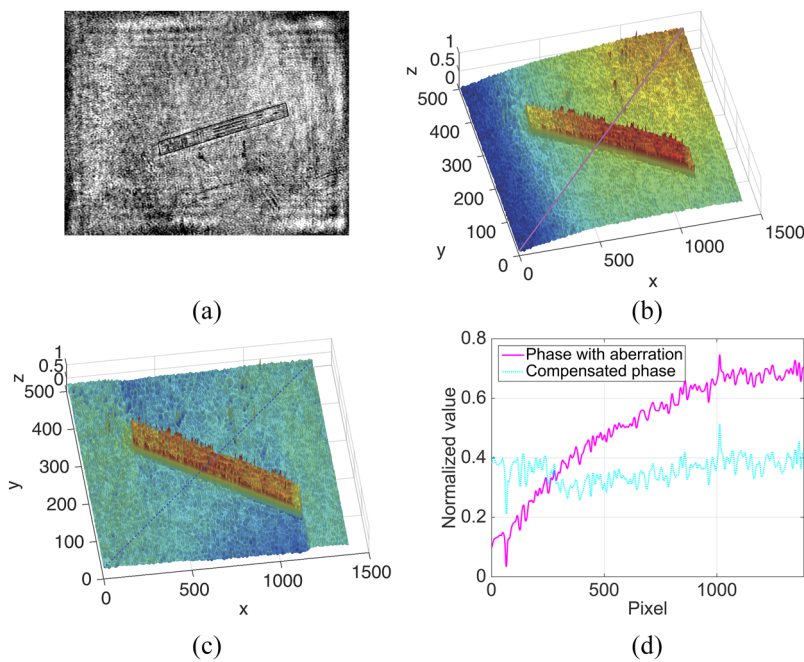

(a)

(b)

(c)

(d)

FIG. 8. (a) Amplitude reconstruction of the groove. (b) Recovered object phase with quadratic aberration. (c) Compensated object phase. (d) Line profile comparison along central lines in (b) (red dashed line) and (c) (blue solid line).

(a)

(b)

(c)

(d)

FIG. 9. (a) Amplitude reconstruction of the circuit. (b) Recovered object phase with quadratic aberration. (c) Compensated object phase. (d) Line profile comparison along central lines in (b) (red dashed line) and (c) (blue solid line).
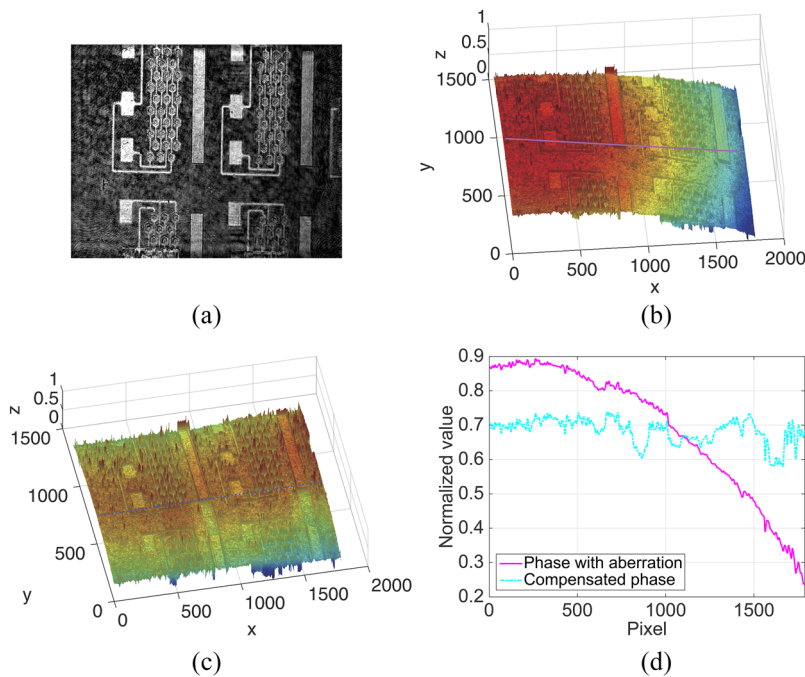
quadratic aberration is not totally removed. As such, the proposed method is utilized to compensate the second-order aberration. Figure 8 shows the amplitude reconstruction of the same groove. Figures 8(b) and 8(c) show the aberrated and aberration-free object phase maps, respectively. The existence and removal of quadratic surface are clearly demonstrated in Fig. 8(d). A similar example of imaging the microcircuit, as shown in Fig. 9, also supports our method.

IV. SUMMARY

To conclude, a numerical method is proposed in this paper for automatically compensating aberrations in phase-contrast imaging using DHM. By formulating the aberration fitting as an inverse problem and by adopting the ℓ_1-norm as the objective function and regularization, an accurate aberration surface can be approximated. As such, by subtracting the estimated aberration surface from the original phase image, the true object phase image can then be recovered for visualization and quantitative measurement. Simulated and experimental results of multiple samples are demonstrated to verify the efficacy of the proposed method in quantitative phase-contrast imaging.

Despite the outperformance and automation of the proposed method here, it has a limitation that more efforts should be engaged in the future. Since solving an ℓ_1-norm-based optimization problem (~10 s) requires more time than that of the ℓ_2-norm (~1 s), this method has a lower computational efficiency (ten times slower) than the least-squares method. As such, for real-time applications such as particle tracking or live cell imaging, this method can only be employed in an offline fashion. Future directions of the reported approach include studies of the cause that makes the optimization slow. We will try faster optimization algorithms or software

packages like the homotopy method or the MOSEK optimization suite to accelerate the computation of the proposed method.

REFERENCES

[1]U. Schnars, C. Falldorf, J. Watson, and W. Jüptner, *Digital Holography and Wavefront Sensing: Principles, Techniques and Applications* (Springer, 2015).
[2]Z. Ren, H. K.-H. So, and E. Y. Lam, "Fringe pattern improvement and super-resolution using deep learning in digital holography," IEEE Trans. Ind. Inf. **15**, 6179 (2019).
[3]F. Merola, P. Memmolo, L. Miccio, R. Savoia, M. Mugnano, A. Fontana, G. D'ippolito, A. Sardo, A. Iolascon, A. Gambale *et al.*, "Tomographic flow cytometry by digital holography," Light: Sci. Appl. **6**, e16241 (2017).
[4]E. Y. Lam, X. Zhang, H. Vo, T.-C. Poon, and G. Indebetouw, "Three-dimensional microscopy and sectional image reconstruction using optical scanning holography," Appl. Opt. **48**, H113–H119 (2009).
[5]Z. Ren, N. Chen, and E. Y. Lam, "Extended focused imaging and depth map reconstruction in optical scanning holography," Appl. Opt. **55**, 1040–1047 (2016).
[6]Z. Ren, Z. Xu, and E. Y. Lam, "Phase aberration compensation in digital holographic microscopy using regression analysis," in *OSA Topical Meeting on Applied Industrial Optics: Spectroscopy, Imaging and Metrology* (Optical Society of America, 2018), p. JTh3B–5.
[7]E. Sánchez-Ortiga, P. Ferraro, M. Martínez-Corral, G. Saavedra, and A. Doblas, "Digital holographic microscopy with pure-optical spherical phase compensation," J. Opt. Soc. Am. A **28**, 1410–1417 (2011).

[8] A. I. Doblas, E. Sánchez-Ortiga, M. Martínez-Corral, G. Saavedra, and J. Garcia-Sucerquia, "Accurate single-shot quantitative phase imaging of biological specimens with telecentric digital holographic microscopy," J. Biomed. Opt. **19**, 046022 (2014).

[9] C. Trujillo, R. Castañeda, P. Piedrahita-Quintero, and J. Garcia-Sucerquia, "Automatic full compensation of quantitative phase imaging in off-axis digital holographic microscopy," Appl. Opt. **55**, 10299–10306 (2016).

[10] W. Qu, C. O. Choo, V. R. Singh, Y. Yu, and A. Asundi, "Quasi-physical phase compensation in digital holographic microscopy," J. Opt. Soc. Am. A **26**, 2005–2011 (2009).

[11] A. Doblas, D. Hincapie-Zuluaga, G. Saavedra, M. Martínez-Corral, and J. Garcia-Sucerquia, "Physical compensation of phase curvature in digital holographic microscopy by use of programmable liquid lens," Appl. Opt. **54**, 5229–5233 (2015).

[12] D. Deng, J. Peng, W. Qu, Y. Wu, X. Liu, W. He, and X. Peng, "Simple and flexible phase compensation for digital holographic microscopy with electrically tunable lens," Appl. Opt. **56**, 6007–6014 (2017).

[13] W. Qu, Y. Yu, C. O. Choo, and A. Asundi, "Digital holographic microscopy with physical phase compensation," Opt. Lett. **34**, 1276–1278 (2009).

[14] T. Colomb, J. Kühn, F. Charriere, C. Depeursinge, P. Marquet, and N. Aspert, "Total aberrations compensation in digital holographic microscopy with a reference conjugated hologram," Opt. Express **14**, 4300–4306 (2006).

[15] P. Ferraro, S. De Nicola, A. Finizio, G. Coppola, S. Grilli, C. Magro, and G. Pierattini, "Compensation of the inherent wave front curvature in digital holographic coherent microscopy for quantitative phase-contrast imaging," Appl. Opt. **42**, 1938–1946 (2003).

[16] I. Choi, K. Lee, and Y. Park, "Compensation of aberration in quantitative phase imaging using lateral shifting and spiral phase integration," Opt. Express **25**, 30771–30779 (2017).

[17] T. Colomb, F. Montfort, J. Kühn, N. Aspert, E. Cuche, A. Marian, F. Charrière, S. Bourquin, P. Marquet, and C. Depeursinge, "Numerical parametric lens for shifting, magnification, and complete aberration compensation in digital holographic microscopy," J. Opt. Soc. Am. A **23**, 3177–3190 (2006).

[18] J. Di, J. Zhao, W. Sun, H. Jiang, and X. Yan, "Phase aberration compensation of digital holographic microscopy based on least squares surface fitting," Opt. Commun. **282**, 3873–3877 (2009).

[19] T. Colomb, E. Cuche, F. Charrière, J. Kühn, N. Aspert, F. Montfort, P. Marquet, and C. Depeursinge, "Automatic procedure for aberration compensation in digital holographic microscopy and applications to specimen shape compensation," Appl. Opt. **45**, 851–863 (2006).

[20] S. Liu, Q. Lian, Y. Qing, and Z. Xu, "Automatic phase aberration compensation for digital holographic microscopy based on phase variation minimization," Opt. Lett. **43**, 1870–1873 (2018).

[21] L. Miccio, D. Alfieri, S. Grilli, P. Ferraro, A. Finizio, L. De Petrocellis, and S. Nicola, "Direct full compensation of the aberrations in quantitative phase microscopy of thin objects by a single digital hologram," Appl. Phys. Lett. **90**, 041104 (2007).

[22] C. Zuo, Q. Chen, W. Qu, and A. Asundi, "Phase aberration compensation in digital holographic microscopy based on principal component analysis," Opt. Lett. **38**, 1724–1726 (2013).

[23] H. Cui, D. Wang, Y. Wang, J. Zhao, and Y. Zhang, "Phase aberration compensation by spectrum centering in digital holographic microscopy," Opt. Commun. **284**, 4152–4155 (2011).

[24] J. Min, B. Yao, S. Ketelhut, C. Engwer, B. Greve, and B. Kemper, "Simple and fast spectral domain algorithm for quantitative phase imaging of living cells with digital holographic microscopy," Opt. Lett. **42**, 227–230 (2017).

[25] D. Deng, W. Qu, W. He, Y. Wu, X. Liu, and X. Peng, "Off-axis tilt compensation in common-path digital holographic microscopy based on hologram rotation," Opt. Lett. **42**, 5282–5285 (2017).

[26] D. Deng, W. Qu, W. He, X. Liu, and X. Peng, "Phase aberration compensation for digital holographic microscopy based on geometrical transformations," J. Opt. **21**, 1–7 (2019).

[27] H. N. D. Le, M. S. Kim, and D.-H. Kim, "Comparison of singular value decomposition and principal component analysis applied to hyperspectral imaging of biofilm," in *IEEE Photonics Conference* (IEEE, 2012), p. 6–7.

[28] T. Nguyen, V. Bui, V. Lam, C. B. Raub, L.-C. Chang, and G. Nehmetallah, "Automatic phase aberration compensation for digital holographic microscopy based on deep learning background detection," Opt. Express **25**, 15043–15057 (2017).

[29] Z. Ren, Z. Xu, and E. Y. Lam, "End-to-end deep learning framework for digital holographic reconstruction," Adv. Photonics **1**, 016004 (2019).

[30] D. L. Donoho, "Compressed sensing," IEEE Trans. Inf. Theory **52**, 1289–1306 (2006).

[31] E. J. Candès and M. B. Wakin, "An introduction to compressive sampling," IEEE Signal Process. Mag. **25**, 21–30 (2008).

[32] A. C. Chan, K. K. Tsia, and E. Y. Lam, "Subsampled scanning holographic imaging (SuSHI) for fast, non-adaptive recording of three-dimensional objects," Optica **3**, 911–917 (2016).

[33] M. Grant and S. Boyd, "CVX: Matlab software for disciplined convex programming, version 2.1," http://cvxr.com/cvx, 2014.

[34] Z. Ren, Z. Xu, and E. Y. Lam, "Learning-based nonparametric autofocusing for digital holography," Optica **5**, 337–344 (2018).

[35] T. Nguyen, G. Nehmetallah, C. Raub, S. Mathews, and R. Aylo, "Accurate quantitative phase digital holographic microscopy with single-and multiple-wavelength telecentric and nontelecentric configurations," Appl. Opt. **55**, 5666–5683 (2016).